RSC Advances

PAPER

View Article Online
View Journal | View Issue

Cite this: *RSC Adv.*, 2017, **7**, 46738

Graphene decorated MoS_2 for eosin Y-sensitized hydrogen evolution from water under visible light

Xing Liu, †*[ab] Lanhua Zhao,†[c] Hua Lai,[b] Yanyan Wei,[b] Guihua Yang,[b] Shuangfeng Yin *[a] and Zhengji Yi[b]

Received 15th August 2017
Accepted 24th September 2017

DOI: 10.1039/c7ra09009a

rsc.li/rsc-advances

Some two-dimensional nanomaterials, such as graphene and molybdenum disulfide, are presently being intensively investigated due to their excellent and unique performances. In the field of photocatalysis, MoS_2 is considered as a promising alternative to noble metal Pt for the hydrogen evolution reaction (HER). However, its poor electrical conductivity restricts its catalytic activity in the HER. In this work, MoS_2 was modified with graphene (G) by a simple hydrothermal method. The prepared G/MoS_2 composite was characterized by X-ray diffraction (XRD), Fourier transform infrared spectroscopy (FTIR) and scanning electron microscopy (SEM). The results show that graphene modification does not influence the crystal phase of MoS_2, but makes the latter more dispersed. The HER performance of G/MoS_2 was evaluated using eosin Y (EY) as a photosensitizer, and triethanolamine (TEOA) as a sacrificial electron donor under visible-light irradiation (λ > 420 nm, 250 W high pressure Hg lamp as light source). The EY sensitized G/MoS_2 composite displays enhanced hydrogen evolution in terms of not only activity but also stability. The average HER activity (9.1 μmol h^{-1}) is three times that of EY sensitized pure MoS_2 over 10 h. It is believed that the incorporation of graphene enhances the charge transfer ability and retards the self-degradation path of $EY^{\bullet -}$, ultimately improving the HER.

1. Introduction

Photocatalytic water splitting into hydrogen, an ideal green energy carrier, by using sunlight is an attractive and sustainable solution to global energy and environmental problems.[1–3] To perform the hydrogen evolution reaction, the photocatalytic system usually consists of a highly efficient photosensitizer (PS), a hydrogen evolution catalyst and a sacrificial electron donor. There have been a large number of reports on Ru complexes as PSs.[4–6] Compared with transition metal complexes, organic dyes (without metals) are usually less expensive and more readily available. Xanthenes, including eosin Y(EY), rosebengal, erythrosin B, appear to be one kind of potential organic dyes that can be used as PSs for the photoreduction of water.[7–13] Unfortunately, there is an instability problem of the dyes in these hydrogen production systems. This must limit the practical application of dye sensitization. The instability may be due to their own high chemical reactivity, taking EY for an instance, reductive quenching product $EY^{\bullet -}$ of excited EY (^{3}EY*) which forms in the photocatalytic hydrogen systems, can undergo debromination reaction to decrease the sensitization activity of EY.[14,15] It should be a good strategy for enhancing stability of the dye to transfer the electron of $EY^{\bullet -}$ by an excellent electron acceptor including catalyst.

As catalysts, they should provide highly active sites for hydrogen formation and reduce the overpotential of hydrogen evolution significantly. Some noble metals, such as Pt, have been fully proven to be an effective cocatalyst/catalyst for this reaction.[14–16] However, the scale-up application of the Pt-based catalysts is still hard at present on account of their scarceness and high-cost. Therefore, the exploration of alternatives consisting solely of earth-abundant elements as well as having highly activity is an important topic.

Molybdenum disulfide (MoS_2) has been investigated in several fields including lithium ion batteries, photoelectrochemical solar cells, biosensors, super lubricants, photodetectors, catalysts, and so on, due to its unique chemical and physical properties.[17–21] Recently, MoS_2 has been reported to be used as a hydrogen evolution (co-)catalyst, but generally speaking, its activity is still low compared to Pt.[22–27] Surface modification of MoS_2 is a feasible means to improve its photoactivity.

As another typical two-dimensional nanomaterial, graphene has been attracting many interests due to its outstanding mechanical, thermal, optical, and electrical properties and wide

[a]College of Chemistry and Chemical Engineering, Hunan University, Changsha, 410082, People's Republic of China. E-mail: sf_yin@hnu.edu.cn

[b]Key Laboratory of Functional Organometallic Materials of College of Hunan Province, College of Chemistry and Material Science, Hengyang Normal University, Hengyang, 421008, People's Republic of China. E-mail: liuxing1127@sina.com

[c]Institue of Pathogenic Biolog, Hunan Provincical Key Laboratory for Special Pathogens Prevention and Control, University of South China, Hengyang, 421001, People's Republic of China

† These authors contributed equally to this work.

applications.[28–33] Surface modification of MoS_2 with graphene (or its oxide) have been demonstrated to enhance the photo-induced charge transfer.[34–41] However, very few works have paid attention to dye sensitized the MoS_2/graphene composites, especially the stability issue for hydrogen evolution from water.

In this work, MoS_2 was modified with graphene by a simple hydrothermal method and EY sensitized graphene/MoS_2 exhibits improved not only activity but also stability of hydrogen production compared to EY sensitized MoS_2 in the presence of triethanolamine (TEOA) as a sacrificial electron donor. This visible-light-driven hydrogen production system without noble metals is expected to contribute toward the development and practical application of photocatalytic technology.

2. Experimental

2.1 Preparation of graphene oxide and reduced graphene oxide

All the chemicals were of analytical grade and were used without further purification. Graphene oxide (denoted as GO) was synthesized by the modified Hummers method according to our previous work.[42] In a typical process, natural graphite (1.0 g) and $NaNO_3$ (0.50 g) were mixed with 23 mL of concentrated H_2SO_4 (98%) in an ice bath (≤4 °C), and the mixture was stirred for 20 min, then 6.0 g of $KMnO_4$ was added within 60 min. The reaction system was kept at room temperature for 2 h, subsequently the suspension was rapidly heated to 95 °C and kept for 30 min, after that, the cold mixture (≤1 °C) of distilled water (100 mL) and H_2O_2 (10 mL) was added and the system immediately became yellow-brown, the resulting mixture was filtrated and washed with distilled water and absolute ethanol until the filtrate is neutral and no SO_4^{2-} (determined with saturated $BaCl_2$ solution) in it. The solid was dried in an oven at 80 °C and GO was obtained.

GO was reduced by a chemical method with hydrazine hydrate ($N_2H_4 \cdot H_2O$) as reductive agent. 0.3 g of GO powder was dissolved in 200 mL distilled water by sonication for 1 h to form GO aqueous solution, then 0.6 g of KOH and 10 mL of $N_2H_4 \cdot H_2O$ was added into above solution under continuous stirring, and then the reaction system kept refluxed at 98 °C for 12 h. Finally, the suspension was cooled and washed with distilled water and ethanol several times, and dried in vacuum at 60 °C. The obtained reduced graphene oxide was abbreviated as G.

2.2 Preparation of graphene decorated MoS_2

The graphene decorated MoS_2 nanohybrid (G/MoS_2) was synthesized by a simple hydrothermal reaction. Typically, a given of as-prepared G powders were dispersed into 50 mL of H_2O under sonication. After that, 5.0 mmol of sodium molybdate ($Na_2MoO_4 \cdot 2H_2O$) and thioacetamide (NH_2CSNH_2) were dissolved into the above suspensions under stirring, and then the mixture was transferred into a 100 mL Teflon-lined autoclave and heated in an oven at 180–220 °C for 16 h. The solid products were collected by filtration, washed carefully with water and ethanol for several times, and dried in a vacuum oven at 50 °C for 6 h. For comparison, the blank samples of MoS_2 were prepared in the absence of G under the same experimental conditions. The G/MoS_2 and MoS_2 catalyst for photocatalytic hydrogen production were grinded in an agate mortar before using.

2.3 Photocatalytic hydrogen generation

Photocatalytic reaction was performed in a 190 mL Pyrex cell with a side flat window. A 250 W high pressure Hg lamp was used as the light source, which was equipped with a cutoff filter (λ > 420 nm) to remove the radiation below 420 nm. The IR fraction of the beam was removed by a cool water filter to ensure illumination of visible light only. In a typical reaction, 0.10 g of G/MoS_2 or MoS_2 was added into 80.0 mL aqueous solution containing TEOA (9.5×10^{-2} mol L^{-1}) and a given concentration EY, whose pH was adjusted to 7.0 with HCl. Before photoreaction, the catalyst was dispersed in an ultrasonic bath for 5 min and high-pure N_2 gas was bubbled through the reaction mixture for 30 min to remove oxygen completely. The top of the cell was sealed with a silicone rubber septum. Sampling was made intermittently through the septum during experiments. The amount of generated hydrogen was determined on a gas chromatograph (TCD, 13X molecular sieve column, N_2 gas carrier).

2.4 Characterization and instruments

X-ray diffraction (XRD) studies were carried out using a Bruker D8 ADVANCE polycrystalline X-ray diffractometer with nickel-filtered Cu Kα radiation as the X-ray source (λ = 0.15406 nm) at a scan rate of 0.05°. The Fourier transform infrared (FTIR) spectra were recorded in transmission mode from 400 to 4000 cm^{-1} at a resolution of 8 cm^{-1} on a Nicolet Magna 560 IR spectrometer using the KBr pellet technique. Scanning electron microscopy (SEM) images were taken on a EVO-10 (Carl Zeiss AG, Germany) working at 30 kV, the samples were mounted onto carbon adhesive pads attached to aluminum stubs. The Brunauer–Emmett–Teller (BET) specific surface areas were determined on an ASAP 2020 (Micromeritics Instruments, USA) nitrogen adsorption apparatus.

3. Results and discussion

3.1 Characterization of the catalysts

Fig. 1 shows the XRD patterns of the as-synthesized G/MoS_2 and MoS_2. The diffraction peaks located at 2θ = 14.0°, 33.4°, 39.8°, 49.4°, 59.3°, 69.9°, could be perfectly indexed to 2H–MoS_2 (JCPDS 37-1492).[43,44] No other impurities phases are detected within the instrument detection limit, which indicates a pure MoS_2 hexagonal phase is formed. No characteristic diffraction peaks of graphene can be observed in G/MoS_2 sample probably because the amount of graphene is low as well as its diffraction intensity is relatively low. The strongest peak at 2θ = 14.0° corresponds to (002) crystal plane of the hexagonal phase, indicating a typical lamellar structure along the *c* axis. The FWH values of (002) peak are 1.91°and 1.62° for G/MoS_2 and MoS_2, respectively. The peak intensity of G/MoS_2 decreases and its

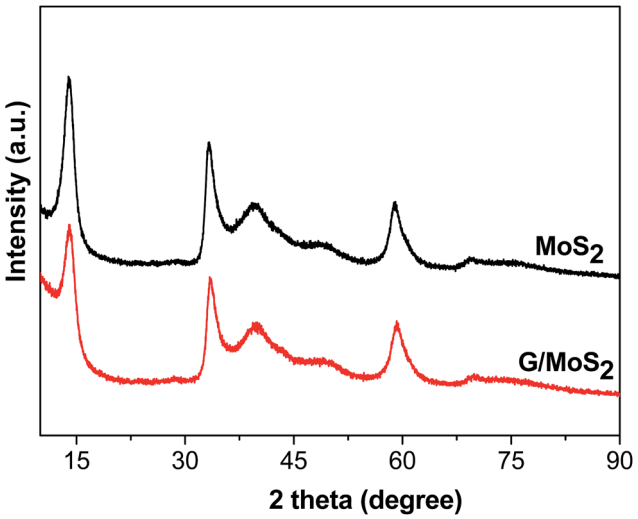

Fig. 1 XRD patterns of G/MoS_2 and MoS_2.

FWH broadens, indicating that the MoS_2 crystallite size becomes smaller after graphene modification.

Fig. 2 shows FT-IR spectra of G/MoS_2, MoS_2, GO and G. The characteristic bands of GO are observed at 1047, 1092 cm^{-1} (alkoxy C–O stretching), 1200 cm^{-1} (phenolic C–OH stretching), 1399 cm^{-1} (carboxyl O–H stretching), 1625 cm^{-1} (C=C skeleton vibrations of graphitic domains), 1710 cm^{-1} (C=O stretching vibrations of carboxyl or carbonyl groups) and 3400 cm^{-1}(–OH bending vibration).[30,45] While the intensities of these oxygen-containing functional groups decrease remarkably in G sample, suggesting that GO is nearly reduced by hydrazine. MoS_2 exhibits a weak "S–Mo–S" absorption band (stretching vibrations) at 460 cm^{-1} approximately.[40,46] The above bands of G and MoS_2 can be observed in G/MoS_2 sample. The vibration band around 2350 cm^{-1} characterizes CO_2 (C=O=C stretching) from the air due to our tests were directly conducted under the atmosphere.

As shown in Fig. 3, MoS_2 is composed of sphere-like clusters and the cluster consists of many thin nanosheets, which is beneficial for the separation of photo-generated carriers. The MoS_2 clusters are stacked together, implying that a significant aggregation occurs. The surface of G sheets (Fig. 3b) are very glossy and has a characteristic wrinkle, the sheets possess planar domains (sp^2 π-conjugated network) and bending domains (sp^3 regions, composed of lattice defects, oxygen groups and dangling bonds).[31] In G/MoS_2 sample (Fig. 3c), MoS_2 clusters are tightly intertwined with graphene sheets, and the intimate contact makes the electronic interaction between MoS_2 and graphene possible. The statistical particle size distributions of MoS_2 and G/MoS_2 were shown in Fig. 3d and e, the average diameter of MoS_2 nanoparticles is 200 ± 50 nm, and it is 150 ± 50 nm for G/MoS_2 nanoparticles. The decrease in average diameter of MoS_2 reveals that they also become more dispersed, which is in agreement with the XRD results. It means that the G decoration can promote the nucleation of MoS_2 but suppress the aggregation of MoS_2 clusters, this is beneficial to hydrogen generation reaction.

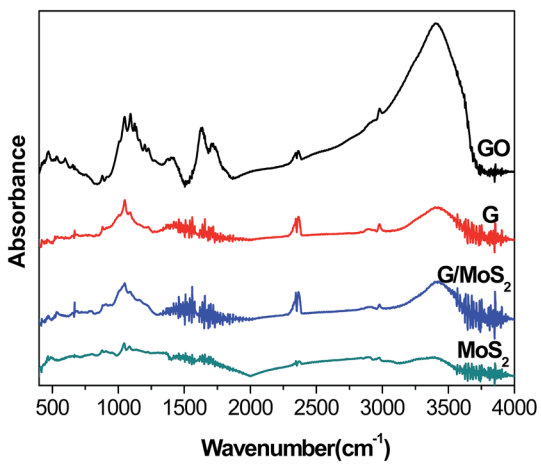

Fig. 2 FT-IR spectra of G/MoS_2, MoS_2, GO and G.

3.2 Dye sensitized hydrogen generation

A noble-metal-free hydrogen production system was constructed with the as-prepared G/MoS_2 as a catalyst, eosin Y as a photosensitizer, and TEOA as a sacrificial electron donor. It is observed from Fig. 4 that G, EY-G (EY sensitized G) and G/MoS_2 systems show negligible photocatalytic H_2 evolution activity, suggesting that both MoS_2 and EY are indispensable in our reaction system. And the EY-MoS_2 (EY sensitized MoS_2) system has a remarkable activity under the same experimental conditions. However, the amount of hydrogen generation from EY-G/MoS_2 (EY sensitized G/MoS_2) system within 2 h irradiation is near twice of that from EY-MoS_2 system. The result indicates that the graphene modification can markedly enhance the sensitized activity for hydrogen generation. Besides, as shown in Fig. 5, the activity of EY-MoS_2 system decreases to very low level after 5 h irradiation while EY-G/MoS_2 system keeps almost constant activity for hydrogen generation within 10 h irradiation, suggesting that the stability of EY-G/MoS_2 system is enhanced compared with EY-MoS_2 system, and the average HER activity (9.1 μmol h^{-1}) is about three times of that from EY sensitized pure MoS_2 (3.1 μmol h^{-1}) within 10 h. It can be explained as follows:[44] (I) graphene could improve the transfer of the photogenerated electrons in the dye species to the edges of MoS_2 and then react with adsorbed H^+ ions to form H_2. (II) The high concentration of electrons between the MoS_2 layer and the graphene layer could greatly enhance the electronic conductivity of composites. (III) MoS_2 becomes more dispersed in the presence of graphene, meaning more active sites for H_2 evolution. Therefore the activities of composites are improved significantly.

The average rate of hydrogen production not high, the possible reasons include: firstly, the light source in our experiments was a 250 W high pressure Hg lamp (equipped with a cutoff filter ($\lambda > 420$ nm)), compared with xenon lamp, its light intensity was very low, so the photocatalytic activity is limited. Secondly, the overpotential for direct hydrogen evolution at MoS_2 active sites is high, thus the rate is relatively slow

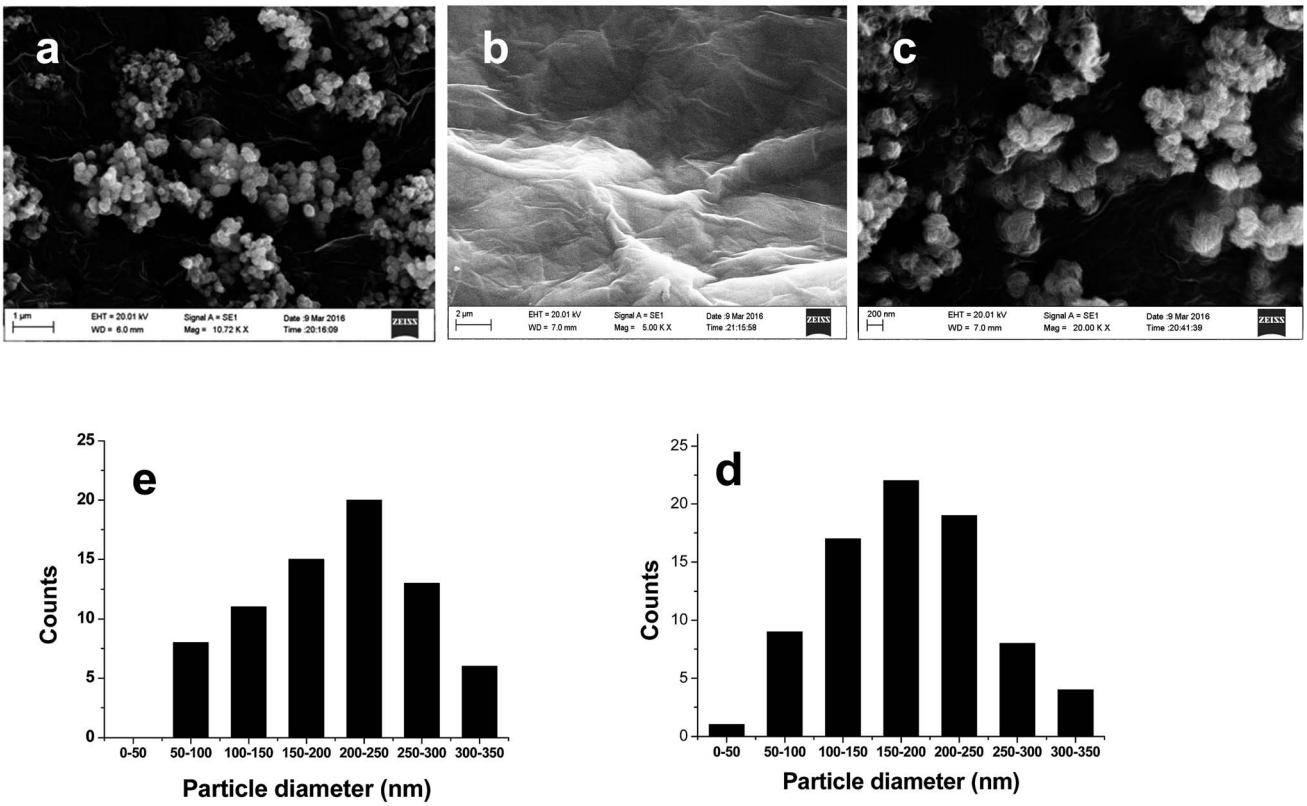

Fig. 3 SEM images of (a) MoS_2, (b) G and (c) G/MoS_2, particle size distribution of (d) MoS_2 and (e) G/MoS_2.

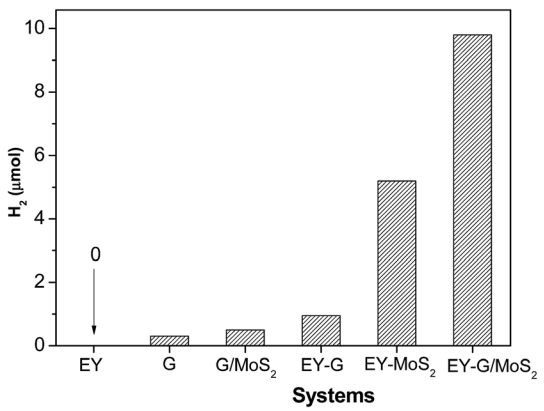

Fig. 4 Photocatalytic H_2 production of various systems. Conditions: 0.10 g catalyst, 2.0 $\times$ 10^{-3} mol L^{-1} TEOA, light source: 250 W high pressure Hg lamp, λ > 420 nm, irradiation time 2 h.

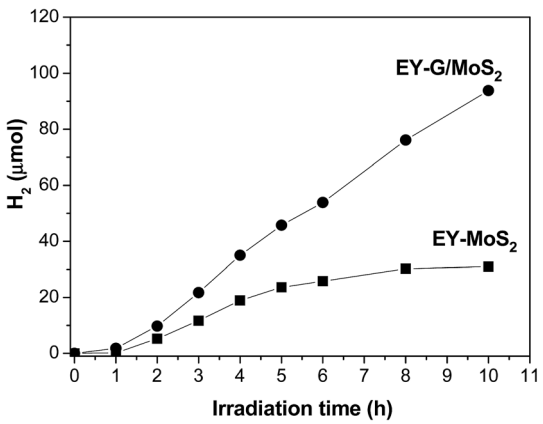

Fig. 5 Time courses of photocatalytic H_2 production of EY sensitized G/MoS_2 and MoS_2. The conditions as Fig. 4.

compared to some others with noble metals which can reduces this overpotential.

It is generally believed that, in EY sensitized hydrogen generation system, the charge transfer is mainly undertaken by ^{3}EY*, which comes from singlet state through intersystem crossing after EY is excited by visible light irradiation. Previous works have demonstrated that ^{3}EY* is prevailingly quenched reductively by electron donor TEOA to form radical $EY^{\bullet-}$ anion in photochemically driven electron-transfer step.[15,47,48] $EY^{\bullet-}$ radicals have two dominating quenching paths: (I) injects its surplus electron into photocatalyst to reduce H+(H_2O). (II) self-degradation, that is, C–Br bonds of $EY^{\bullet-}$ usually cleave very fast, leading to its photobleaching and the loss of photoactivity.[15,49] Obviously, self-degradation path of $EY^{\bullet-}$ is detrimental to our targeted HER. The higher electrical conductivity of photocatalyst (electron acceptor) is, the stronger its electron transfer ability will be. The electron transfer from $EY^{\bullet-}$ to photocatalyst should take place highly effectively because the introduction of graphene indeed enhances the electrical conductivity of the G/MoS_2 composite. This electron transfer from $EY^{\bullet-}$ can compete

favorably with its debromination. So, in other words, debromination of $EY^{\bullet -}$ is inhibited to some extent. $EY^{\bullet -}$ radicals injects its surplus electron into G/MoS_2 and transforms itself into original EY. As a result, the sensitization activity and stability of G/MoS_2 improved. Based on the above discussions, a probable mechanism of the photosensitized hydrogen production is proposed as shown in Fig. 6.

Some related reaction conditions were investigated. Fig. 7 described the effect of initial G concentration on hydrogen evolution. When G concentration increased from 0 to 0.25 mg mL^{-1}, a positive impact on hydrogen evolution was observed. This may be ascribed to the increase of G promoting electron transfer as well as dispersion of MoS_2. When GO concentration further increased to 0.50 mg mL^{-1}, there was a negative impact on hydrogen evolution, because the introduction of a large percentage of black graphene leads to shielding of the MoS_2 active sites, called a "shielding effect". Therefore, a GO concentration of 0.25 g L^{-1} was found to be optimal. When G concentrations are 0, 0.125, 0.25, 0.50 mg mL^{-1}, the BET specific surface areas of the prepared G/MoS_2 samples are 19.7, 24.4, 27.1, 31.6 m^2 g^{-1}, respectively. This suggests that introduction of graphene increases the specific surface areas of G/MoS_2 composites, which is in agreement with the SEM and XRD analyses. Since the heterogeneous photocatalysis is a surface-dependent reaction, a large surface area should provide more surface active sites for the adsorption of reactants, making the photocatalytic HER more efficient. Moreover, $EY^{\bullet -}$ species preferentially transfer their electrons to G and then to active sites of MoS_2, leading to spatially separation of photogenerated charges, which could be understood by comparing their energy levels. Since the reductive potential of $EY^{\bullet -}$ is −0.8 V (*vs.* NHE) whilst the work function of G is 0.16 V and the conduction band potential of MoS_2 is 0.20 V. The electron transfer from the $EY^{\bullet -}$ to G then to MoS_2 is thermodynamically feasible. This enhanced electron transfer is also demonstrated by numerous reports.[16,35,43,44]

The effect of hydrothermal temperature on photocatalytic hydrogen evolution is shown in Fig. 8. When hydrothermal temperature alters from 180 to 220 °C, the MoS_2 prepared at 200 °C shows the best hydrogen evolution activity. It can be easily understood that higher temperature is conductive to the crystallization of MoS_2 as well as further reduction of graphene, while the average size of MoS_2 nanosheets increases with increased hydrothermal temperature. As a photocatalyst, usually, MoS_2 should have small size as well as high crystallinity, as a result of trade-off of the two kinds of factors, a optimal hydrothermal temperature at 200 °C occurs in our experiments.

Fig. 9 shows the impact of EY concentration on hydrogen evolution. The photocatalytic activities increases first and then declines with increase of EY concentration, and reaches a maximum at 3.1×10^{-4} mol L^{-1}. If no dye is added, only a little evolved hydrogen is observed, this demonstrates that hydrogen generation is indeed driven by dye sensitization. When concentration of EY increases from 0 to 3.1×10^{-4} mol L^{-1}, the antenna effect of dye to absorb light is boosted, more and more

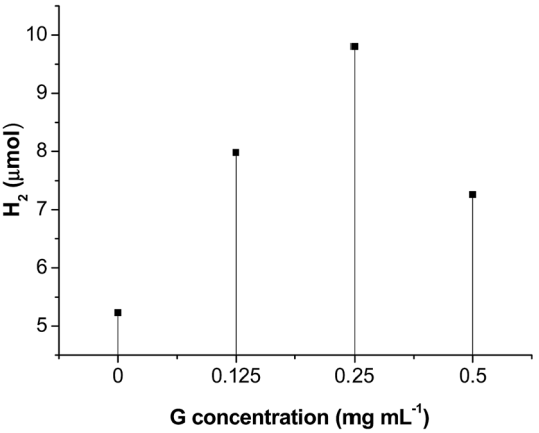

Fig. 7 Effect of initial G concentration on hydrogen evolution of EY sensitized G/MoS_2. Conditions: 200 °C hydrothermal temperature, 3.1×10^{-4} mol L^{-1} EY, 2.0×10^{-3} mol L^{-1} TEOA, visible light (λ > 420 nm) irradiation for 2 h.

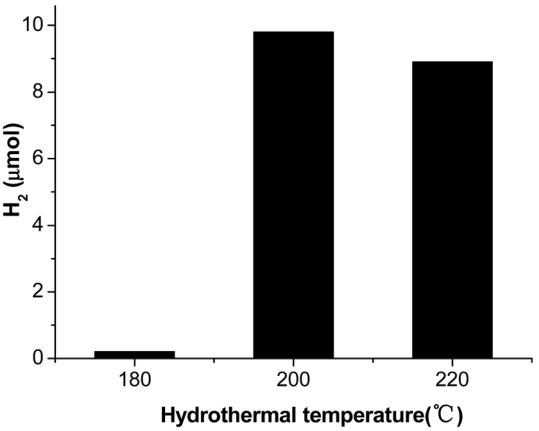

Fig. 8 Effect of hydrothermal temperature on hydrogen evolution of EY sensitized G/MoS_2. Conditions: 0.25 mg mL^{-1}initial G concentration, 3.1×10^{-4} mol L^{-1} EY, 2.0×10^{-3} mol L^{-1} TEOA, visible light (λ > 420 nm) irradiation for 2 h.

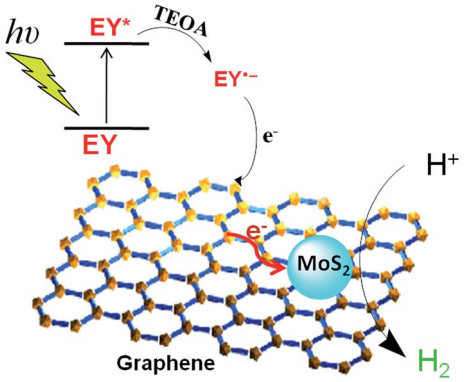

Fig. 6 Schematic representation of probable mechanism of photosensitized hydrogen production. Noted that EY*, $EY^{\bullet -}$, TEOA represent the triplet excited state of eosin Y, the radical anion of eosin Y and triethanolamine, respectively.

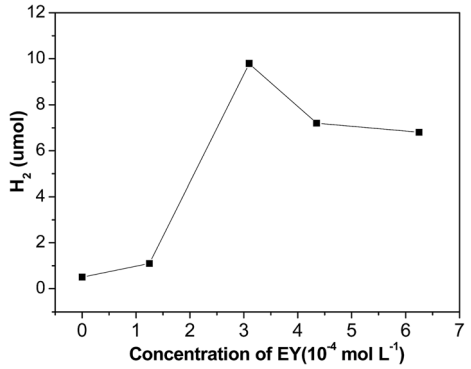

Fig. 9 Effect of EY concentration on hydrogen evolution of EY sensitized G/MoS_2. Conditions: 0.25 mg mL^{-1}initial G concentration, 200 °C hydrothermal temperature, 3.1 × 10^{-4} mol L^{-1} EY, 2.0 × 10^{-3} mol L^{-1} TEOA, visible light (λ > 420 nm) irradiation for 2 h.

radical $EY^{\bullet -}$ anion generates, thus the hydrogen evolution is enhanced. Nevertheless, when the concentration of EY is extremely high, many free dye molecules in solution absorb the input light but would not contribute to hydrogen evolution. Moreover, greater collisional deactivation of the ^{3}EY* excited state happens due to serried dye molecules, so the activity of hydrogen evolution would not rise.

4. Conclusions

In summary, MoS_2 was modified with graphene by a simple hydrothermal method, the graphene modification does not influence the crystal phase of MoS_2, but makes it more dispersed. EY sensitized G/MoS_2 composite displays enhanced photocatalytic hydrogen generation in terms of not only activity but also stability. It is believed that the incorporation of graphene enhances the charge transfer abilities and retards the self-degradation path of $EY^{\bullet -}$, ultimately improving the photocatalytic H_2 evolution. This kind of noble-metal-free dye-G/MoS_2 system has great potential for photocatalytic H_2 production under visible light irradiation.

Conflicts of interest

There are no conflicts to declare.

Acknowledgements

The authors are grateful for financial support of this research by the National Natural Science Foundation of China (21603065, 41773133), the Hunan Provincial Natural Science Foundation of China (2016JJ6013), the China Postdoctoral Science Foundation (2017M612547), the Scientific Research Fund of Hunan Provincial Education Department (17C1383), the Project of Science and Technology Bureau of Hengyang City (2016KJ67), the Aid Programs for Science and Technology Innovative Research Team on Functional Organometallic Compounds in Higher Educational Institutions of Hunan Province, and the Key Discipline of Material Physics and Chemistry of Hunan Province.

References

1 A. Kudo and Y. Miseki, *Chem. Soc. Rev.*, 2009, **38**, 253–278.
2 X. Liu, J. Iocozzia, Y. Wang, X. Cui, Y. H. Chen, S. Q. Zhao, Z. Li and Z. Q. Lin, *Energy Environ. Sci.*, 2017, **10**, 402–434.
3 M. D. Bhatt and J. S. Lee, *RSC Adv.*, 2017, **7**, 34875–34885.
4 T. Y. Peng, K. Dai, H. B. Yi, D. N. Ke, P. Cai and L. Zan, *Chem. Phys. Lett.*, 2008, **460**, 216–219.
5 X. H. Zhang, U. Veikko, J. Mao, P. Cai and T. Y. Peng, *Chem.–Eur. J.*, 2012, **18**, 12103–12111.
6 E. Bae and W. Choi, *J. Phys. Chem. B*, 2006, **110**, 14792–14799.
7 X. H. Zhang, T. Y. Peng and S. S. Song, *J. Mater. Chem. A*, 2016, **4**, 2365–2402.
8 J. Willkomm, K. L. Orchard, A. Reynal, E. Pastor, J. R. Durrant and E. Reisner, *Chem. Soc. Rev.*, 2016, **45**, 9–23.
9 W. J. Jiao, Y. Q. Wu, G. X. Lu and H. W. Jing, *RSC Adv.*, 2016, **6**, 29538–29544.
10 Z. G. Mou, Y. P. Dong, S. J. Li, Y. K. Du, X. M. Wang, P. Yang and S. D. Wang, *Int. J. Hydrogen Energy*, 2011, **36**, 8885–8893.
11 W. Y. Zhang, Y. X. Li and S. Q. Peng, *J. Mater. Chem. A*, 2017, **5**, 13072–13078.
12 J. Y. Xu, Y. X. Li and S. Q. Peng, *Int. J. Hydrogen Energy*, 2015, **40**, 353–362.
13 J. Y. Xu, Y. X. Li, S. Q. Peng, G. X. Lu and S. B. Li, *Phys. Chem. Chem. Phys.*, 2013, **15**, 7657–7665.
14 X. Liu, Y. X. Li, S. Q. Peng and H. Lai, *Acta Phys.-Chim. Sin.*, 2015, **31**, 612–626.
15 X. Liu, Y. X. Li, S. Q. Peng, G. X. Lu and S. B. Li, *Int. J. Hydrogen Energy*, 2013, **38**, 11709–11719.
16 Z. Li, Q. S. Wang, C. Kong, Y. Q. Wu, Y. X. Li and G. X. Lu, *J. Phys. Chem. C*, 2015, **119**, 13561–13568.
17 J. Chen, S. L. Li, Q. Xu and K. Tanaka, *Chem. Commun.*, 2002, 1722–1723.
18 S. Y. Tai, C. J. Liu, S. W. Chou, F. S. S. Chien, J. Y. Lin and T. W. Lin, *J. Mater. Chem.*, 2012, **22**, 24753–24759.
19 J. Xu, T. F. He, L. Q. Chai, L. Qiao, X. Q. Zhang, P. Wang and W. M. Liu, *Phys. Chem. Chem. Phys.*, 2017, **9**, 8161–8173.
20 S. Mukherjee, R. Maiti, A. Midya, S. Das and S. K. Ray, *ACS Photonics*, 2015, **2**, 760–768.
21 Q. Wang and J. H. Li, *J. Phys. Chem. C*, 2007, **111**, 1675–1682.
22 D. Merki and X. Hu, *Energy Environ. Sci.*, 2011, **4**, 3878–3888.
23 B. Han and Y. H. Hu, *Energy Sci. Eng.*, 2016, **4**, 285–304.
24 T. T. Jia, M. M. J. Li, L. Ye, S. Wiseman, G. L. Liu, J. Qu, K. Nakagawa and S. C. E. Tsang, *Chem. Commun.*, 2015, **51**, 13496–13499.
25 J. Choi, D. A. Reddy, N. S. Han, S. Jeong, S. Hong, D. P. Kumar, J. K. Song and T. K. Kim, *Catal. Sci. Technol.*, 2017, **7**, 641–649.
26 M. C. Yin, C. J. Wu, F. F. Jia, L. J. Wang, P. F. Zheng and Y. T. Fan, *RSC Adv.*, 2016, **6**, 75618–75625.
27 G. Malekshoar and A. K. Ray, *Chem. Eng. Sci.*, 2016, **152**, 35–44.
28 A. K. Geim, *Science*, 2009, **324**, 1530–1534.

29 W. Y. Zhang, Y. X. Li, S. Q. Peng and X. Cai, *Beilstein J. Nanotechnol.*, 2014, **5**, 801–811.
30 W. Y. Zhang, Y. X. Li and S. Q. Peng, *ACS Appl. Mater. Interfaces*, 2016, **8**, 15187–15195.
31 C. Mattevi, G. Eda, S. Agnoli, S. Miller, K. A. Mkhoyan, O. Celik, D. Mastrogiovanni, G. Granozzi, E. Garfunkel and M. Chhowalla, *Adv. Funct. Mater.*, 2009, **19**, 2577–2583.
32 X. Z. Gong, G. Z. Liu, Y. S. Li, D. Y. W. Yu and W. Y. Teoh, *Chem. Mater.*, 2016, **28**, 8082–8118.
33 B. Cecconi, N. Manfredi, T. Montini, P. Fornasiero and A. Abbotto, *Eur. J. Org. Chem.*, 2016, **2016**, 5194–5215.
34 R. K. Biroju, D. Das, R. Sharma, S. Pal, L. P. L. Mawlong, K. Bhorkar, P. K. Giri, A. K. Singh and T. N. Narayanan, *ACS Energy Lett.*, 2017, **2**, 1355–1361.
35 Y. G. Li, H. L. Wang, L. M. Xie, Y. Y. Liang, G. S. Hong and H. J. Dai, *J. Am. Chem. Soc.*, 2011, **133**, 7296–7299.
36 T. T. Jia, A. Kolpin, C. S. Ma, R. C.-T. Chan, W. M. Kwok and S. C. E. Tsang, *Chem. Commun.*, 2014, **50**, 1185–1188.
37 Z. H. Deng, L. Li, W. Ding, K. Xiong and Z. D. We, *Chem. Commun.*, 2015, **51**, 1893–1896.
38 X. Li, L. Zhang, X. B. Zang, X. M. Li and H. W. Zhu, *ACS Appl. Mater. Interfaces*, 2016, **8**, 10866–10873.
39 Y. X. Li, H. Wang and S. Q. Peng, *J. Phys. Chem. C*, 2014, **118**, 19842–19848.
40 K. Pramoda, U. Gupta, I. Ahmad, R. Kumar and C. N. R. Rao, *J. Mater. Chem. A*, 2016, **4**, 8989–8994.
41 L. Zhang, L. Sun, S. Liu, Y. H. Huang, K. W. Xu and F. Ma, *RSC Adv.*, 2016, **6**, 60318–60326.
42 X. Liu, L. H. Zhao, H. Lai, S. Li and Z. Y. Yi, *J. Chem. Technol. Biotechnol.*, 2017, **92**, 2417–2424.
43 S. X. Min and G. X. Lu, *J. Phys. Chem. C*, 2012, **116**, 25415–25424.
44 K. Chang, Z. W. Mei, T. Wang, Q. Kang, S. X. Ouyang and J. H. Ye, *ACS Nano*, 2014, **8**, 7078–7087.
45 Q. Li, B. D. Guo, J. G. Yu, J. R. Ran, B. H. Zhang, H. J. Yan and J. R. Gong, *J. Am. Chem. Soc.*, 2011, **133**, 10878–10884.
46 W. S. Nin, G. Z. Bian and Y. L. Fu, *J. Zhejiang Univ. Technol.*, 2001, **3**, 213–216.
47 X. Liu, Y. X. Li, S. Q. Peng, G. X. Lu and S. B. Li, *Photochem. Photobiol. Sci.*, 2013, **12**, 1903–1910.
48 T. Lazarides, T. McCormick, P. W. Du, G. G. Luo, B. Lindley and R. Eisenberg, *J. Am. Chem. Soc.*, 2009, **131**, 9192–9194.
49 J. D. Hong, Y. B. Wang, J. S. Pan, Z. Y. Zhong and R. Xu, *Nanoscale*, 2011, **3**, 4655–4661.